A Single-Molecule Atomic Force Microscopy Study of PARP1 and PARP2 Recognition of Base Excision Repair DNA Intermediates

Maria V. Sukhanova[1,†], Loic Hamon[2,†], Mikhail M. Kutuzov[1], Vandana Joshi[2], Sanae Abrakhi[2], Ioana Dobra[2], Patrick A. Curmi[2], David Pastre[2] and Olga I. Lavrik[1]

1 - Institute of Chemical Biology and Fundamental Medicine (ICBFM) SB RAS, *8 Lavrentiev Avenue, Novosibirsk 630090, Russia*
2 - SABNP, *Univ Evry, INSERM U1204, Université Paris-Saclay, 91025 Evry, France*

Correspondence to Olga I. Lavrik: *lavrik@niboch.nsc.ru*
https://doi.org/10.1016/j.jmb.2019.05.028
Edited by Achillefs Kapanidis

Abstract

Nuclear poly(ADP-ribose) polymerases 1 and 2 (PARP1 and PARP2) catalyze the synthesis of poly(ADP-ribose) (PAR) and use NAD^+ as a substrate for the polymer synthesis. Both PARP1 and PARP2 are involved in DNA damage response pathways and function as sensors of DNA breaks, including temporary single-strand breaks formed during DNA repair. Consistently, with a role in DNA repair, PARP activation requires its binding to a damaged DNA site, which initiates PAR synthesis. Here we use atomic force microscopy to characterize at the single-molecule level the interaction of PARP1 and PARP2 with long DNA substrates containing a single damage site and representing intermediates of the short-patch base excision repair (BER) pathway. We demonstrated that PARP1 has higher affinity for early intermediates of BER than PARP2, whereas both PARPs efficiently interact with the nick and may contribute to regulation of the final ligation step. The binding of a DNA repair intermediate by PARPs involved a PARP monomer or dimer depending on the type of DNA damage. PARP dimerization influences the affinity of these proteins to DNA and affects their enzymatic activity: the dimeric form is more effective in PAR synthesis in the case of PARP2 but is less effective in the case of PARP1. PARP2 suppresses PAR synthesis catalyzed by PARP1 after single-strand breaks formation. Our study suggests that the functions of PARP1 and PARP2 overlap in BER after a site cleavage and provides evidence for a role of PARP2 in the regulation of PARP1 activity.

Introduction

DNA of living organisms is subjected to the action of genotoxic agents of either endogenous or exogenous origin [1]. The resulting DNA damage, if left unrepaired, can lead to mutations, premature cell death, or malignant cell transformation [2,3]. DNA repair plays a central role in the maintenance of genome integrity in all forms of life [4]. Base excision repair and single-strand break repair (BER and SSBR) pathways are responsible for the repair of damaged DNA bases, apurinic/apyrimidinic (AP) sites and SSBs [5]. According to the currently accepted model of mammalian BER, the processing of damaged DNA can proceed through three subpathways and involves not only DNA repair enzymes but also numerous accessory factors [6,7]. Among them, nuclear poly(ADP-ribose) polymerases 1 and 2 (PARP1 and PARP2) catalyze the synthesis of poly(ADP-ribose) [PAR] using NAD^+ as a substrate [8–10]. PARP1 and PARP2 recognize damaged DNA and synthesize long and branched PAR chains covalently attached to themselves or acceptor proteins [11,12]. PARP1 and PARP2 are considered as primary sensors of DNA breaks and are implicated in the recognition of radiation-induced or temporary SSBs formed during DNA repair [8,12,13]. Disruption of both PARP genes results in early embryonic mortality, providing strong evidence for shared functions of these proteins in biological processes including the DNA damage response [14]. A *PARP1* or *PARP2* gene knockout or knockdown increases the sensitivity of cells to ionizing radiation or monofunctional alkylating agents treatment, indicating functional redundancy between these proteins in the repair of damaged

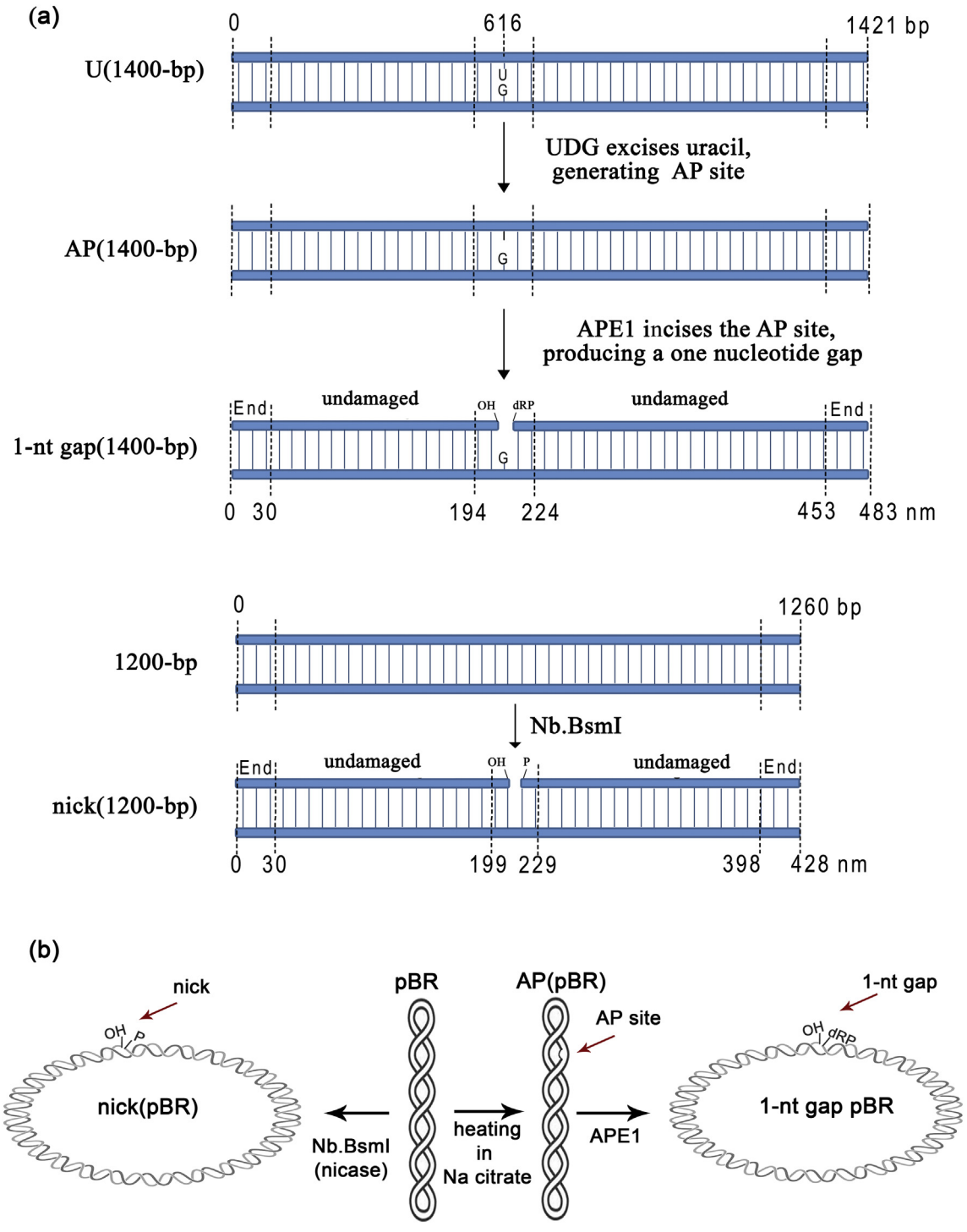

Fig. 1. Simplified scheme of long DNA substrates containing single-strand damage used in this study. (a) Schematic presentation of the linear DNA substrates used in AFM experiments U(1400-bp) DNA, AP(1400-bp), 1-nt gap (1400-bp), 1200-bp, and nick(1200-bp). The DNA substrates were treated with UDG, APE1 or Nb.BsmI to produce AP site, 1-nt gap, or nick, respectively. (b) Schematic presentation of the plasmid DNAs used in this study. The plasmid DNAs were treated with Na citrate, (Na citrate + APE1) or Nb.BsmI to produce AP site, 1-nt gap, or nick, respectively.

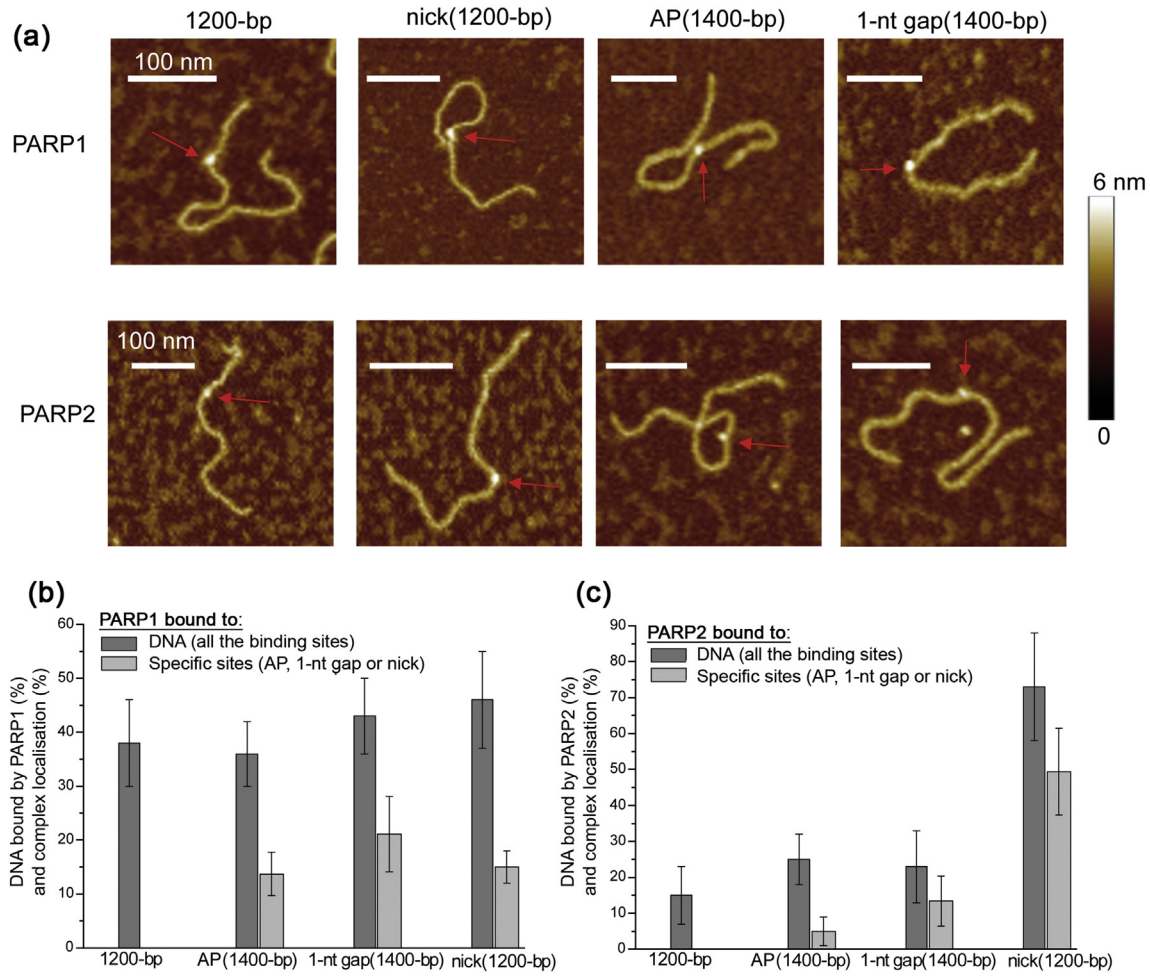

Fig. 2. AFM imaging and analysis of PARP–DNA complexes: site-specific binding of PARP1 and PARP2 to an AP site, 1-nt gap, or nick. (a) AFM images of complexes of PARP1 (top row) or PARP2 (bottom row) with undamaged DNA (1200-bp) or with site-specific DNA damage (nick, AP site, or 1-nt gap). DNA substrates (1 nM) were incubated with 2 nM PARP1 or 3.5 nM PARP2 and imaged by AFM in air. The scale bar represents 100 nm; the Z scale represents 6 nm. (b) Fractional occupancy (%) of a DNA fragment and specific site (AP site, 1-nt gap, or nick) by PARP1. The numbers of DNA molecules analyzed: 187 for 1200-bp, 134 for nick(1200-bp), 247 for AP(1400-bp), and 218 for 1-nt gap(1400-bp). The results represent mean ± SD of three independent experiments. (c) Fractional occupancy (%) of a DNA fragment and specific site (AP site, 1-nt gap, or nick) by PARP2. The numbers of DNA molecules analyzed: 147 for 1200-bp, 89 for nick(1200-bp), 64 for AP(1400-bp), and 179 for 1-nt gap(1400-bp). The results are presented as mean ± SD of three independent experiments.

bases and SSBs [12,14]. Overlapping roles of PARP1 and PARP2 in the recruitment of key SSBR or BER factors, such as XRCC1 and polynucleotide kinase-phosphatase (PNKP), to DNA was also confirmed recently in experiments on PARP1$^{-/-}$, PARP2$^{-/-}$, and PARP1$^{-/-}$PARP2$^{-/-}$ mutant cells under conditions of oxidative stress [15]. Both proteins seem to be involved in BER and SSBR via interaction with repair proteins and DNA repair intermediates [12,16–28]. In the case of PARP1, its interaction with key DNA intermediates in BER, such as AP sites, 1-nucleotide (1-nt) gaps, or nicks, has been detected in crude cell extracts by the photoaffinity labeling technique or $NaBH_4$ cross-linking [18,26–28]. For PARP2, its interaction with BER DNA intermediates has been mainly characterized using systems reconstituted from purified proteins [20,21,29,30]. Both PARPs can modulate BER enzyme activity in *in vitro* reconstituted systems [19–21,26,28]. Nonetheless, the effect of these PARPs on BER seems to be more complex and is not limited to the interaction with repair proteins and binding to DNA intermediates [11,13,31]. Numerous studies indicate that the synthesis of PAR catalyzed by PARPs performs an important function in the regulation of DNA repair [11,32]. PARP1 produces ~90% of PAR formed in the cell, and local PAR synthesis at DNA damage sites is critical for

Table 1. Binding constants (K_D, nM) for specific site[a]

DNA damage site	AP site	1-nt gap	Nick
PARP1	10.4 ± 3.1	5.8 ± 1.7	8.8 ± 1.9
PARP2	62.5 ± 37.5	22.0 ± 10.0	3.1 ± 1.1

[a] Measured by AFM imaging (Fig. 2b and c).

recruitment of BER factors and/or enzymes, such as XRCC1, DNA ligase III, PNKP, and aprataxin, to DNA lesions [33,34]. PARP2 has lower activity than PARP1, and its contribution to overall PAR synthesis in response to DNA damage is ~15%–25% [12,35]. Potentially, the competition of PARP2 with PARP1 for binding to DNA structures appearing during repair may influence their activation and the bulk of PAR production [12,20]. Despite these important advances in understanding of the critical functions of PARP1 and PARP2 in DNA repair, the relative functions and cooperative actions of these proteins in the regulation of BER and SSBR are still obscure [10,36]. PARP1 interacts with BER intermediates starting from AP site formation [18,28]. It has been reported that PARP2 is implicated in late BER steps [10], whereas our previous studies have shown that this protein is able to interact with DNA containing an AP site, which is an early DNA intermediate in the BER pathway [21]. A large number of studies have evaluated the activation of PARP1 and PARP2 by a broad range of short single- or double-stranded oligonucleotides including DNA structures mimicking BER or SSBR intermediates, thus sometimes yielding contradictory data on preferential structures that are more effective in PARP activation [20,21,29,30,37]. Nevertheless, there are still few studies evaluating DNA damage specificity of these enzymes in the context of long DNA substrates [38–41]. The use of long DNA substrates seems to be more relevant to *in vivo* DNA-processing events and allows researchers to discriminate nonspecific protein–DNA binding from single-target-site binding as well as to minimize the influence of DNA ends [41,42].

Here, we focused on characterization of DNA binding and activation of PARP1 and -2 by means of long DNA substrates that represent intermediates of the short-patch BER pathway and contain a single damage site. To gain further insight into the features of PARP1 or PARP2 interaction with these structures, we performed single-molecule imaging with atomic force microscopy (AFM), bulk fluorescence titration, and an assay of PARP automodification activity. The comparison of PARP1 and PARP2 complexes with DNA at the single-molecule level elucidated the features of recognition of DNA damage and PAR synthesis. We demonstrated that PARP1 predominantly binds as a monomer to a 1-nt gap or nick, whereas PARP2 can form dimers with these types of DNA damage. We found that the presence of SSBs is necessary for efficient binding of PARP2 to DNA, which is followed by PARP2 autoPARylation. We also noted that the enzymatic activity and length of PAR produced by PARP2 depend on its initial affinity to the DNA damage site. Although PARP1 activity is influenced by the type of DNA damage, the length of synthesized PAR is only weakly affected by this factor. We showed that the kinetics of PAR synthesis catalyzed by PARP1 on SSB are influenced by PARP2, implying competition between these proteins for their binding. These findings highlight the importance of PARP2 for BER and SSBR and for modulation of PARP1 activity in these processes.

Results

PARP1 and PARP2 show a difference in their affinity for DNA intermediates of short-patch BER

Both PARP1 and PARP2 have been reported to interact with BER DNA intermediates and proteins and can be involved in the repair process from the early stages [12,16–28]. The shared substrate specificity between PARP1 and PARP2 suggests that both proteins may participate in BER regulation [12,20]. Although the interaction of PARP1 and PARP2 with repair intermediates represented by short DNA duplexes has been well studied, there has been no detailed research evaluating the PARP binding to (and activity toward) long DNA substrates.

Fig. 3. AFM imaging and analysis of the distribution of PARP1 and PARP2 in mixture of DNA fragments 1-nt gap(1400-bp) and nick(1200-bp). (a) AFM images of mixture of nick(1200-bp) (red arrows) and an equal amount of 1-nt gap(1400-bp) (blue arrows) after incubation with 4 nM PARP1 (top) or 7 nM PARP2 (bottom) and zoomed-in images (right) of nick(1200-bp) and 1-nt gap (1400-bp) with bound proteins. PARP1 (2) interacts with a DNA nick or gap site (white stars) or with a nonspecific site (white triangles). The scale bar represents 500 or 100 nm; the Z scale represents 7 nm. (b) DNA bound by PARP1 (%) and site-specific localization of protein complex (%) in mixture of DNAs. The numbers of DNA molecules analyzed: 144 and 163 for mixtures of 1-nt gap(1400-bp) and nick(1200-bp), respectively, and 84 and 150 for mixtures of 1-nt gap(1400-bp) and 1200-bp, respectively. The results represent mean ± SD of three independent experiments. (c) DNA bound by PARP2 (%) and site-specific localization of protein complex (%) in mixture of DNAs. The numbers of DNA molecules analyzed: 104 and 121 for mixtures of 1-nt gap(1400-bp) and 1200-bp, respectively, and 102 and 84 for mixtures of 1-nt gap(1400-bp) and nick(1200-bp), respectively. The results represent mean ± SD of three independent experiments.

Here, we focused on the comparative analysis of PARP1 and -2 interactions with single-strand DNA damage, which can be produced as intermediates of the classic short-patch BER pathway involved in the repair of damaged bases and AP sites in DNA [7]. To assess the participation of PARP1 and PARP2 in the interaction with short-patch BER intermediates, we evaluated the affinity of these proteins to an AP site, a 1-nt gap with 3′-OH and 5′-deoxyribose phosphate (dRP), and a nick with 3′-OH and a 5′-phosphate (P) group via previously described AFM- and fluorescence-based DNA–protein binding assays

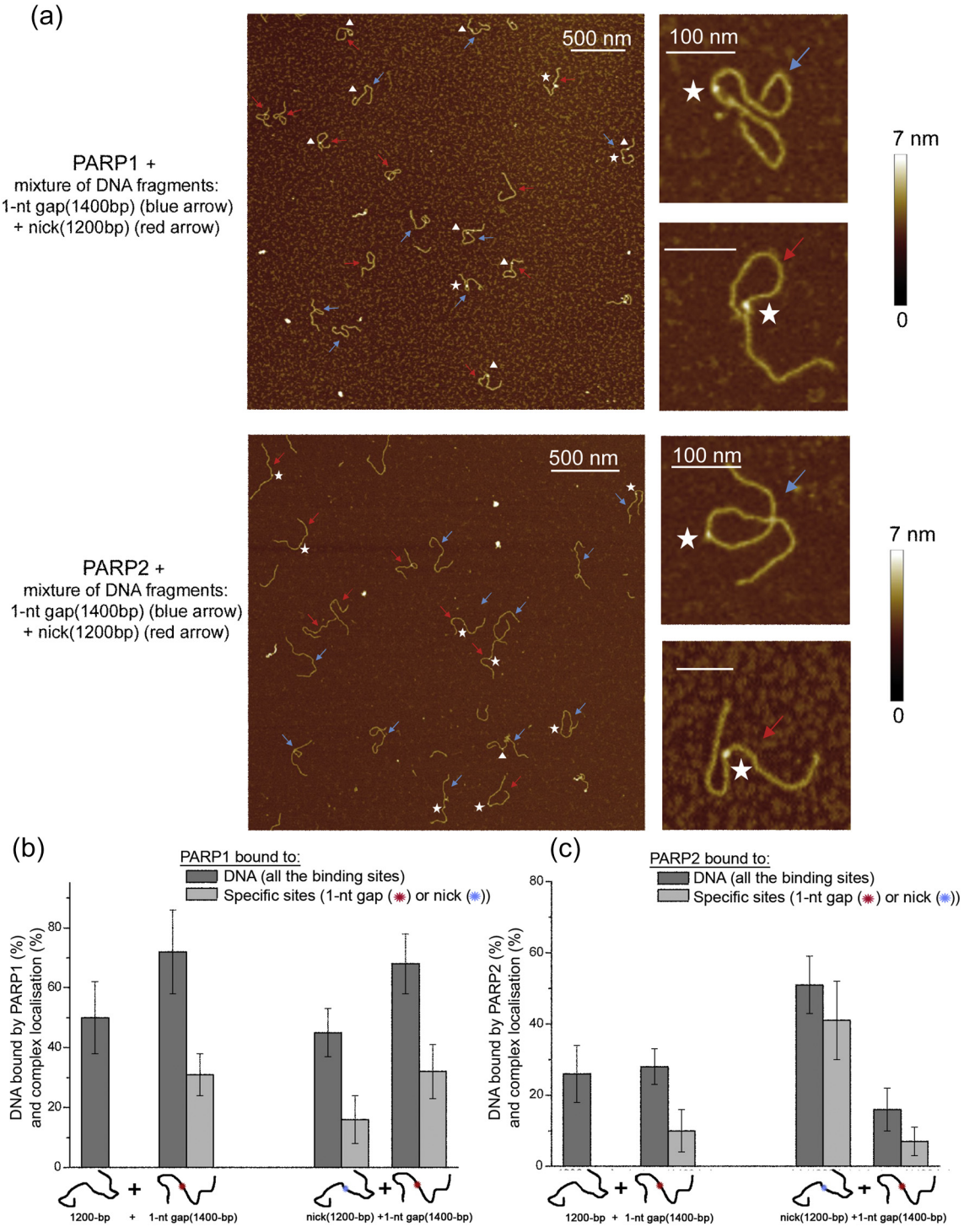

Fig. 3 (*legend on previous page*)

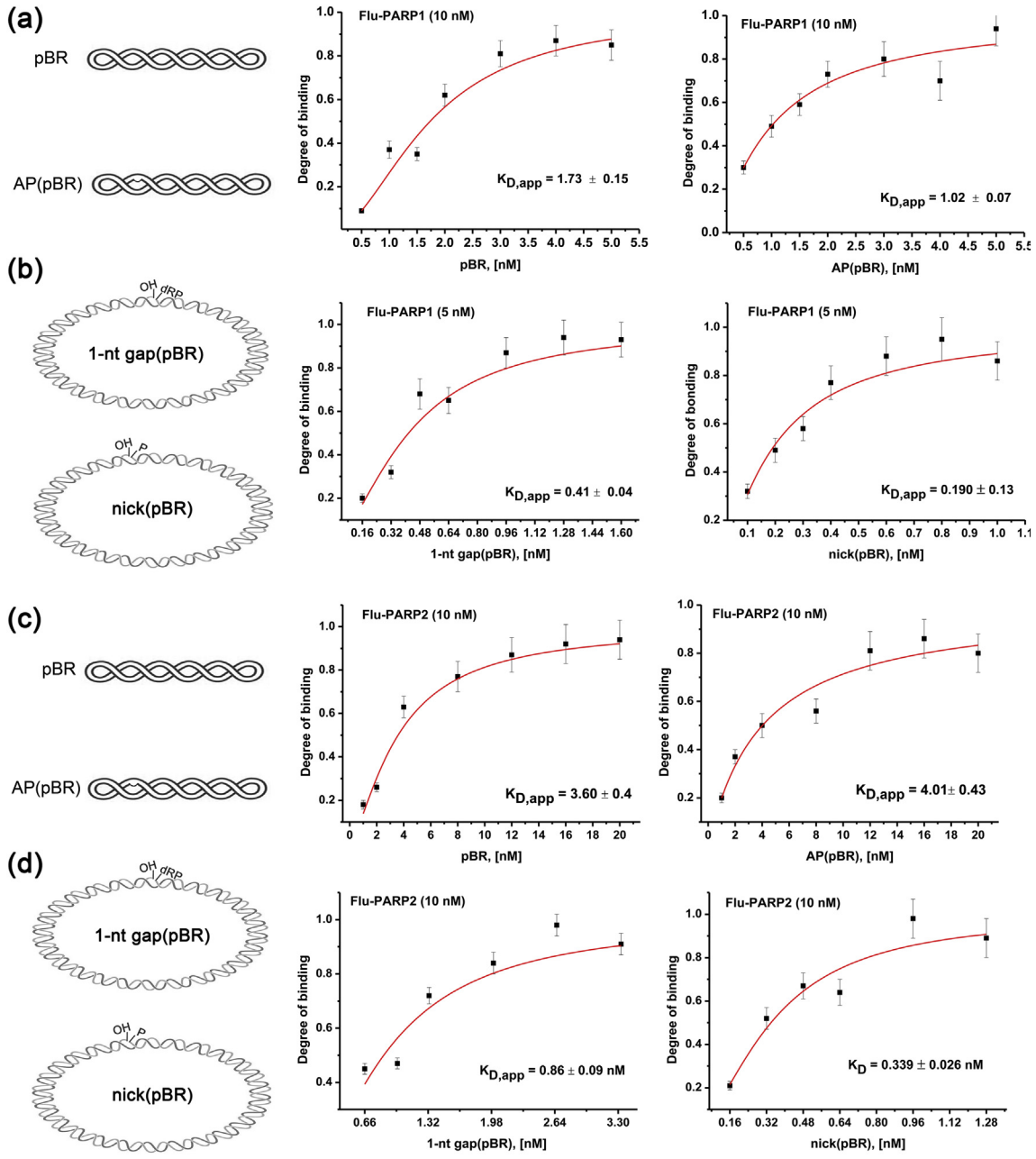

Fig. 4. A fluorescence-based binding assay for quantifying PARP1 (a and b) or PARP2 (c and d) binding to plasmid DNA containing a single-strand DNA damage site (AP site, 1-nt gap, or nick). A fluorescein-labeled protein, Flu-PARP1 or Flu-PARP2, was titrated with various amounts of plasmid DNAs. Bars indicate the standard error of three independent experiments.

[41]. The efficiency of binding of PARP1 and PARP2 to long DNA substrates containing a single DNA damage site was first analyzed by AFM. Three types of DNA substrates, 1400-bp DNA fragments containing either a single AP site [AP (1400-bp)] or a 1-nt gap [1-nt gap(1400-bp)] after nucleotide position 615 (43% from one of the termini) and 1200-bp DNA with a nick in the middle of the chain [nick(1200-bp)] were synthesized to perform the AFM analysis (Fig. 1a). These kinds of BER intermediates can be formed by sequential action of at least three enzymes: UDG, which excises uracil and generates an AP site, apurinic/apyrimidinic endonuclease 1 (APE1), which hydrolyzes the AP site and produces a 1-nt gap flanked by 3′-OH and a 5′-dRP group, and DNA polymerase β, which excises the 5-dRP group and

fills in the 1-nt gap, thereby generating a nick with 3′-OH and a 5′-P group [6]. The treatment of 1200-bp DNA with the nicking endonuclease resulted in production of conventional nicks containing 3′-OH and a 5′-P group mimicking the late BER substrate formed after fill-in DNA synthesis and before DNA ligation (Fig. 1a). The interaction of PARP1 and PARP2 with the long DNA fragment containing a single nick was characterized by us in another study [41]. Here, we used nick(1200-bp) DNA to compare the affinity of these proteins for the nick with the affinity for other types of single-strand damage, like an AP site and 1-nt gap formed during BER. Direct interaction of PARP1 and PARP2 with DNA duplexes representing intermediates of the short-patch pathway of BER has been proved in systems reconstituted with purified proteins or in cell extracts [18,19,21,26,28]. The visualization of protein–DNA complexes by AFM allowed us to analyze the interaction of PARPs with BER-related DNA lesions in detail. At the first step, complexes of PARP1 or -2 with a substrate DNA [AP (1400-bp), 1-nt gap (1400-bp), or nick(1200-bp)] were analyzed by AFM imaging (Fig. 2a). The 1200-bp DNA fragment without single-strand DNA damage served as a negative control (Fig. 1a). Under the applied conditions, we observed that 38% to 48% of each DNA substrate was involved in complex formation with PARP1 (Fig. 2b). It is worth noting that the amount of PARP1–DNA complexes was relatively constant regardless of the appearance of the AP site, 1-nt gap, or nick in DNA (Fig. 2b). Nonetheless, in the case of PARP2, the formation of single-strand DNA damage led to a 1.5- to 5-fold increase in the percentage of DNA fragments that were bound to the protein in comparison with 1200-bp DNA (Fig. 2a and c). Analysis of the position distributions for PARP1 or -2 complexes showed that 30% to 48% of PARP1 and 15% to 69% of PARP2 molecules were located at the specific site (AP site, 1-nt gap, or nick; Fig. 2b and c). Determination of the fractional occupancy as the amount of proteins bound to the AP site, 1-nt gap, or nick helped to calculate site-specific binding constants for PARP1 and -2 (Tables 1 and S1).

A direct comparison of PARP1's affinity values for the DNA damage sites revealed slight differences in the apparent K_D ($K_{D,app}$) values; this protein showed the following ranking of binding affinity: 1-nt gap > nick > AP site. In comparison to PARP1, PARP2 binds efficiently to the nick, and the differences among PARP2 affinity values for the nick, 1-nt gap, and AP site are more pronounced and decrease in the following order: nick ≫ 1-nt gap ≫ AP site. Among the BER-related DNA damage types tested here, PARP2 binds efficiently to an SSB with 3′-OH and 5′-P (nick) formed at the final stage of BER, with the affinity close to that of PARP1 for this type of damage [41]. In particular, the AP site and 1-nt gap were bound by PARP2 with lower affinity relative to PARP1 (Table 1). These data indicate that there is no significant difference in the binding affinity of PARP1 for the AP site, 1-nt gap, or nick, and that PARP2 has an evident binding preference for the nick. To determine directly whether PARPs have a preference for one damage site over the others, we also performed AFM imaging of PARP–DNA complexes formed in mixtures containing equal concentrations, close to 1:1, of two DNA substrates, namely, 1-nt gap(1400-bp) and nick(1200-bp) DNA fragments or 1-nt gap(1400-bp) and 1200-bp DNA fragments (Fig. 3). It should be noted that the use of DNA substrates of different lengths allowed us to distinguish between proteins interacting with 1400-bp or 1200-bp DNA fragments in the same image (Fig. S1a–c). The mixture of two DNAs (containing the 1-nt gap and the 1200-bp fragment without a nick) served as a control in the redistribution analysis (Fig. 3b and c). Using the AFM images, we determined the percentage of DNA molecules bound by PARPs for each type of DNA in the mixtures of the substrates [1200-bp + 1-nt gap (1400-bp) or nick(1200-bp) + 1-nt gap(1400-bp)]. The analysis of AFM images uncovered a significant preference of PARP2 for nicked DNA over the 1-nt gap–containing DNA (Fig. 3c). Thus, ~50% of complexes were formed between PARP2 and nicked DNA (Fig. 3c). Much less of the 1-nt gapped DNAs in the mixture, ~15%, was bound by PARP2. In contrast to PARP2, PARP1 showed a slight preference for binding to the 1-nt gapped DNA over nicked DNA substrates (70% *versus* 43%; Fig. 3b). For all binding assays with a mixture of damaged DNAs, the position of the DNA-bound proteins was also identified (Fig. 3b and c). The analysis of the PARP1 and -2 protein position on the DNA in the mixture of the fragments also uncovered a strong preference of PARP2 to the nick over the 1-nt gap damage site (40% *versus* 4%) and that PARP1 preferentially binds to the 1-nt gap (31% *versus* 16%; Fig. 3b and c).

Thus, these results of a single-molecule assay mean that PARP1 binds with high affinity to an AP site and 1-nt gap, whereas PARP2 has lower affinity for these lesions; however, these proteins have nearly equivalent affinity for the nick site in double-stranded DNA. This finding also suggests that there is an obvious difference between PARP1 and PARP2 in their affinities for DNA intermediates of early stages of the BER pathway.

In addition to the AFM single-molecule binding assay, the interactions of PARP1(2) with a long DNA molecule containing single damage produced by BER enzymes were analyzed by fluorescence titration, under the conditions identical to those in the AFM experiments (Fig. 4). For each PARP1(2)–DNA complex, $K_{D,app}$ was estimated by plotting fluorescence intensity changes of fluorescein-

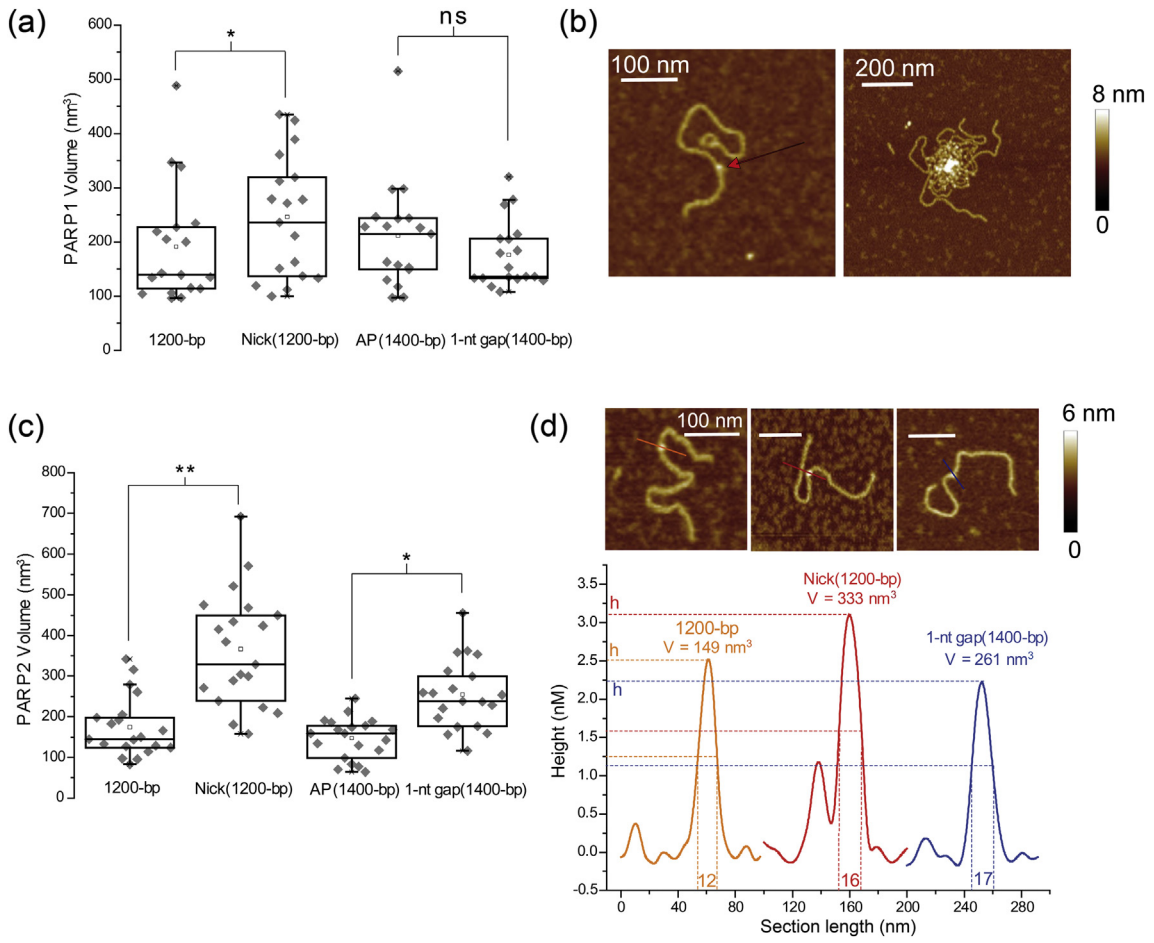

Fig. 5. Oligomeric states of PARP1 and PARP2 molecules bound to undamaged DNA, an AP site, 1-nt gap, or nick. (a) A box plot showing the volume distribution of PARP1 bound to undamaged DNA or to a specific site (nick, AP site, or 1-nt gap). Box charts are formatted as a box (25th to 75th percentiles), vertical bars (5th to 95th percentiles), and data points (diamonds, n = 20 particles) overlapping with the mean value (the empty square) and median value (the horizontal line in the box). $^{**}P < 0.01$, $^{*}P < 0.05$, ns: nonsignificant according to the two-tailed *t* test. (b) AFM images of different structures of PARP1–1200-bp DNA complexes. When a single protein interacts with the DNA (red arrow in the left-hand panel), it is possible to measure both the volume and position of the protein on the DNA molecule. Nonetheless, PARP1 has a tendency to oligomerize and form aggregates in which numerous DNA and protein molecules are embedded and preclude any PARP volume measurements (the zoomed-in image in the right-hand panel). Only isolated complexes were analyzed to create the graph (a). The scale bar represents 100 or 200 nm; the Z scale represents 8 nm. (c) A box plot showing the volume distribution of PARP2 bound to undamaged DNA or a specific site (nick, AP site, or 1-nt gap). Box charts are formatted as a box (25th to 75th percentiles), vertical bars (5th to 95th percentiles), and data points (diamonds, n = 20 particles) overlapping with the mean value (the empty square) and median value (the horizontal line in the box). $^{**}P < 0.01$, $^{*}P < 0.05$, ns: nonsignificant according to the two-tailed *t* test. (d) Top: AFM images of PARP2 bound to 1200-bp DNA (left), a nick site (middle), or 1-nt gap site (right). In comparison with PARP1, the propensity of PARP2 for oligomerization is low, and no aggregates were detected in AFM images. The scale bar represents 100 nm; the Z scale represents 6 nm. Bottom: a cross-section of proteins bound to DNA allowing for determination of protein volume. The height and width at the half height of each peak are indicated on the *y*- and *x*-axes, respectively. Box charts are depicted as a box (25th to 75th percentiles), vertical bars (5th to 95th percentiles), and data points (diamonds, n = 20 particles) overlapping with the mean value (the empty square) and median value (the horizontal line in the box). $^{**}P < 0.01$, $^{*}P < 0.05$, ns: nonsignificant according to the two-tailed *t* test.

labeled proteins owing to complex formation at various DNA concentrations (Fig. 4). For this purpose, we employed undamaged circular plasmid DNA or the ones containing on average one damage per 4361 bp, for example, a supercoiled pBR plasmid with an AP site [AP(pBR)], a circular pBR plasmid with a 1-nt gap [1-nt gap(pBR)], or a nick [nick(pBR)] (Figs. 1b and S2). According to the

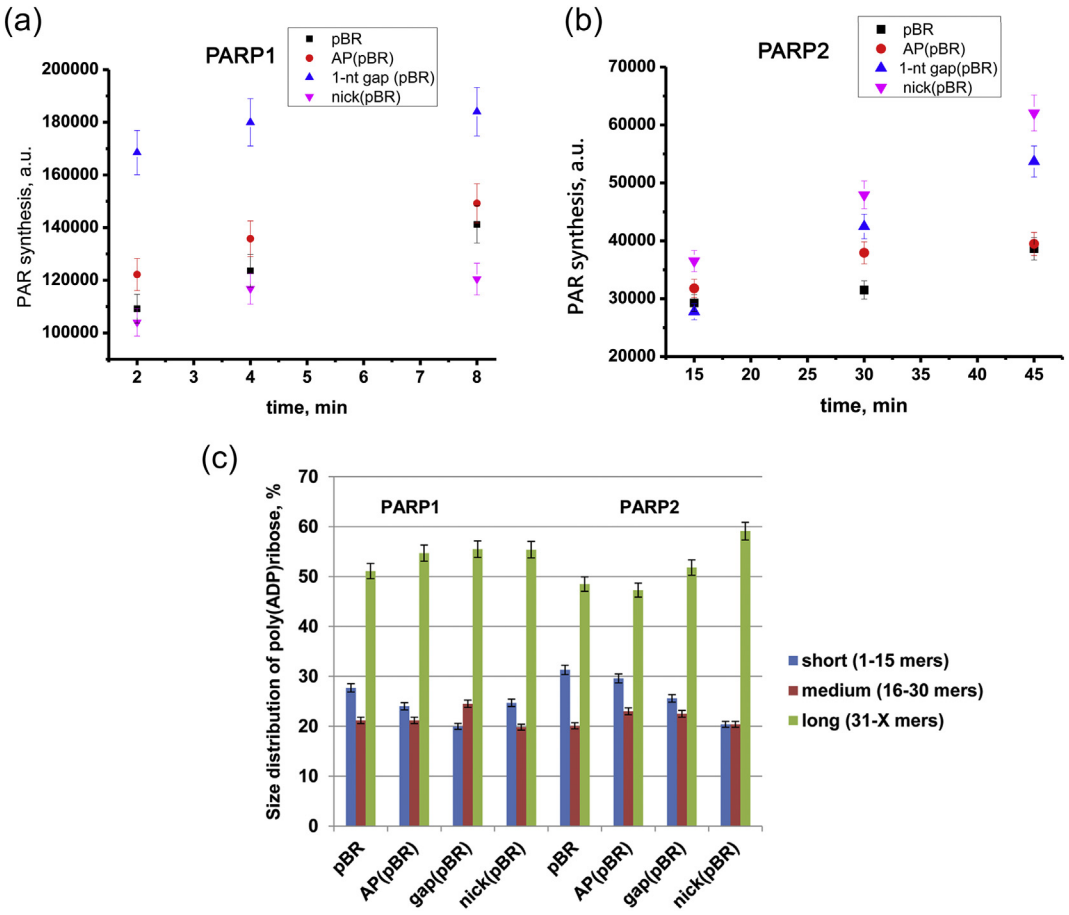

Fig. 6. Analysis of PAR synthesis activity of PARPs in the presence of plasmid DNA containing single-strand DNA damage (AP site, 1-nt gap, or nick). (a, b) The radioactive poly(ADP-ribosyl)ation assay showing time-dependent autoPARylation of PARP1 (a) and PARP2 (b) in the presence pBR, AP(pBR), 1-nt gap(pBR), or nick(pBR). The data are presented as the average of three independent measurements. The graph illustrates quantification of ^{32}P-labeled PAR. The data shown are mean values and standard deviations from three independent experiments including the experiment shown in Fig. S4a and b. (c) Chain length distribution of ADP-ribose polymers synthesized by PARP1 or PARP2 in the presence of plasmid DNA bearing an AP site, 1-nt gap, or nick. The diagram depicts quantification of the ^{32}P-labeled detached PAR shown in Fig. S4c. Quantitative analysis of the PAR chain length expressed as a percentage of short, medium, or long polymers. The values denote the average of three independent measurements.

data, both PARP2 and PARP1 have only small differences in the affinity for AP(pBR) as compared to undamaged pBR (Fig. 4). In agreement with the high-affinity binding of the 1-nt gap and nick *versus* undamaged or abasic sites by PARP2 as revealed by AFM, we observed that the introduction of an SSB resulted in a one-order-of-magnitude increase in the binding affinity of this protein for plasmid DNAs (Fig. 4c and d). For PARP1, the affinity for 1-nt gap-containing or nick-containing DNA was higher too, but the difference between the estimated K_D values for nonbreak and SSB-containing plasmids was $\leq$5-fold (Fig. 4a and b) and higher affinity was detected for nick-containing plasmid DNA. This result somewhat contradicts AFM images of PARP1 complexes with linear DNA (Fig. 2b), which show that the extent of PARP1 binding to DNA was slightly higher for the 1-nt gap than for the nick-containing substrate (Fig. 2b). Thus, K_D values revealed that the affinity of PARP1 and PARP2 was the highest for nick(pBR) followed by 1-nt gap(pBR) and then AP(pBR) and undamaged pBR (the last two affinity values are similar). PARP1 was found to have higher affinity than PARP2 for all the plasmid DNAs tested. This finding could be explained by the fact that PARP1 has higher affinity for undamaged DNA than PARP2 does, which results in a significant contribution of nonspecific DNA binding by PARP1 [41]. Overall, the binding affinity data suggest that the two proteins have pronounced differences in their relative affinities for damaged *versus* undamaged

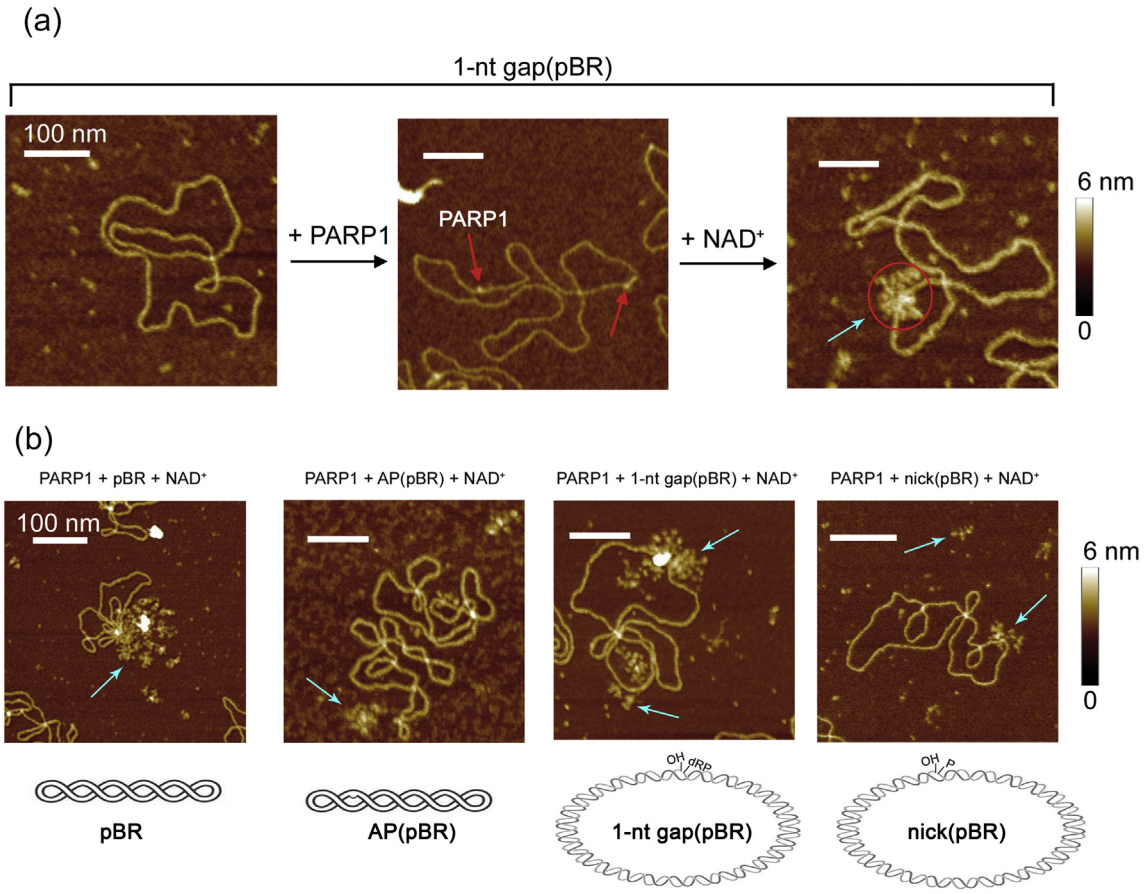

Fig. 7. AFM visualization the shape of PAR polymers synthesized by PARPs in the presence of plasmid DNAs containing single-strand DNA damage (AP site, 1-nt gap, or nick). (a) Large-scale AFM images (left to right) of 1-nt gap plasmid DNA, PARPs bound to DNA and auto-PARylation of PARPs. PARPs (3.5 nM) were incubated with plasmid DNA (0.35 nM) at 37 °C for 30 min in the presence of 100 μM NAD^+. Blue arrow indicates PARylated proteins bound to DNA molecules, and the red circle encloses the PARylated protein bound to DNA. The scale bar represents 100 nm; the Z scale represents 6 nm. (b) Comparative analysis of the shape of PARylated PARP1 in the presence of different DNA substrates. PARP1 (3.5 nM) was incubated with plasmid DNA (0.35 nM) at 37 °C for 30 min in the presence of 100 μM NAD^+. Blue arrows indicate PARylated proteins on the mica surface. The scale bar represents 100 nm; the Z scale represents 6 nm.

DNA substrates; PARP1 and PARP2 have close affinity values for the nick site but differ significantly in their affinity for the 1-nt gap and AP sites.

PARP1 and PARP2 form dimeric complexes at an SSB

Both PARP1 and PARP2 can form and act as dimers at a site of DNA damage [12,30,43–46], although other studies suggest that PARP1 functions as a monomer [47–50]. In this context, the protein volume measurement by AFM can provide additional information on the oligomeric state of PARPs in the complexes with DNA [50,51]. To address this question, we analyzed the AFM volume of PARP1 and PARP2 bound to damage sites (AP site, 1-nt gap, or nick) or undamaged DNA (Figs. 1a and 5). These AFM images contained both free and DNA-bound PARP molecules, and the protein volume distributions of the two forms were studied independently (Figs. 5a, c, and S3). For free proteins detected on a mica surface under the selected conditions, most of PARP1 and PARP2 particles had volumes similar to those expected for the monomer: 208 ± 28 and 142 ± 19 nm^3, respectively (Fig. S3b). This result is consistent with our previous study, where the volume of the free proteins was measured by means of AFM images [41]. It should be pointed out that PARP1 has a tendency for oligomerization that results in formation of small aggregates in which many DNA and protein molecules are embedded (Fig. 5b, right-hand panel). The calculation of volumes as well as analysis of the site-specific binding is impossible in such particles; therefore, they were discarded, and only isolated complexes were taken into account for the volume

determination (Fig. 5b, left-hand panel). The detailed analysis of the protein volume depending on the protein's position along the 1200-bp, nick(1200-bp), AP(1400-bp), or 1-nt gap(1400-bp) DNA fragments indicated that PARP1 binds to undamaged sites, the AP site, and 1-nt gap preferentially as a monomer but is prone to oligomerization, forming dimers at the nick site (Fig. 5a and b). Thus, our results are consistent with other studies, which have evaluated the interaction of PARP1 with long DNA containing an abasic site analog (tetrahydrofuran) using AFM [50]. PARP2 bound as a monomer to undamaged DNA and to an AP site (Fig. 5c and d). PARP2 oligomerization, in which dimers predominate, occurred after its interaction with a 1-nt gap or nick (Fig. 5c). These results suggest that the interaction of PARP2 with a 1-nt gap and nick promotes the formation of PARP2 dimers, and the protein recognizes damaged and undamaged sites in a different way. At the same time, PARP1 is predominantly dimeric only when bound to a nick site. The observed dimerization of PARPs could affect their catalytic activity.

Catalytic activity of PARP1 and PARP2 is dependent on the type of single-strand DNA damage

To characterize DNA-dependent PARP1 and PARP2 activation during BER, it is important to understand how PAR synthesis can be affected by the type of single-strand damage. To analyze PAR synthesis catalyzed by PARP1(2), we performed PARP1 and PARP2 automodification assays in the presence of long DNA substrates bearing one site-specific damage. Because PARP1 and -2 are activated by SSBs and blunt ends in the case of linear DNA substrates, the catalytic activity of these proteins was examined with supercoiled and circular plasmid DNAs [pBR, AP(pBR), 1-nt gap(pBR), and nick(pBR)] (Fig. 1b). At the first step, the PAR synthesis activity of PARP1(2) was evaluated by a standard approach in a polyacrylamide gel electrophoresis (PAGE)-based assay that allows for the measurement of enzymatic activity (Figs. 6a and b, and S4a and b). As expected, the presence of a nick or 1-nt gap in the circular plasmid DNA influenced the PARP1(2) activity (Fig. 6a and b). In contrast, we did not observe noticeable stimulation of PAR synthesis for the AP site–containing pBR *versus* intact pBR for both proteins (Fig. 7a and b). Of note, nick formation did not lead to an increase in PARP1 activity in comparison with the supercoiled DNAs; however, the presence of the 1-nt gap induced stronger protein autoPARylation (Fig. 6a). AFM measurements of the protein volumes revealed that PARP1 interacts with the nick via dimer formation (Fig. 5a). This observation suggests that PARP1's binding in monomeric form to the 1-nt gap leads to its strong autoPARylation, but the dimeric form interacting with the nick is less effective in PAR synthesis (Fig. 6a). These results are consistent with the data indicating that more effective PAR synthesis is catalyzed by PARP1 when the protein acts as a monomer and PAR synthesis likely proceeds via an intramolecular mechanism [52]. In the case of PARP2, the level of its autoPARylation clearly correlated with the increase in the binding affinity of the protein for DNA damage sites tested here (Fig. 6b and Table 1). Nonetheless, an increase in PAR synthesis was observed clearly after longer incubation (30–45 min), indicating a slow rate of PARP2 autoPARylation despite its higher affinity for the 1-nt gap or nick *versus* AP site or undamaged DNA. In addition, AFM analysis revealed PARP2 dimerization upon binding to the 1-nt gap or nick (Fig. 5c), suggesting that the dimers are more efficient in PAR synthesis in the case of PARP2 (Fig. 6b).

To further characterize the features of PAR synthesis when intact DNA (pBR) or plasmids bearing a single type of damage (AP, 1-nt gap, or nick) served as substrates (Fig. 1b), we studied the size of PAR polymers when polymers were detached from protein after chemical treatment [53]. The detached PAR polymers synthesized by PARP1 or PARP2 in the presence of the plasmid substrates were separated by denaturing PAGE and then classified into three groups according to the length distribution: short (1–15mers), medium (16–30mers), and long (>31mers; Figs. 6c and S4c). The length distribution of PAR polymers synthesized by PARP1 for the intact pBR plasmid was estimated as follows: ~28% of short, ~21% of medium, and ~52% of long polymers (Fig. 6c). For PARP1, the introduction of a single AP site, 1-nt gap, or nick into plasmid DNA led to only slight changes: ~3% in the length distribution of PAR in comparison with intact pBR (Fig. 6c). For example, the percentage of short PAR polymers decreased, but production of long chains increased by ~3%. Thus, the presence of a lesion in plasmid DNA mainly modulates the total PARP1 activity but does not significantly change the length distribution of the resulting PAR polymers. For PARP2, the PAR chain length distribution obtained after 45-min incubation for intact DNA was estimated as follows: ~31% of short, ~22% of medium, and ~47% of long polymers. This distribution was close to those obtained after 15-min incubation of PARP1 with the same substrate (Fig. 6c). In contrast to PARP1, SSB formation in the plasmid DNA caused a reduction in the amount of PAR in the fractions of short and medium polymers, shifting the PAR production catalyzed by PARP2 toward longer polymers.

In addition, we performed the morphology analysis of shape of PAR polymers synthesized by the proteins (Fig. 7). For this purpose, plasmid DNAs were incubated with PARP1 or PARP2 in the

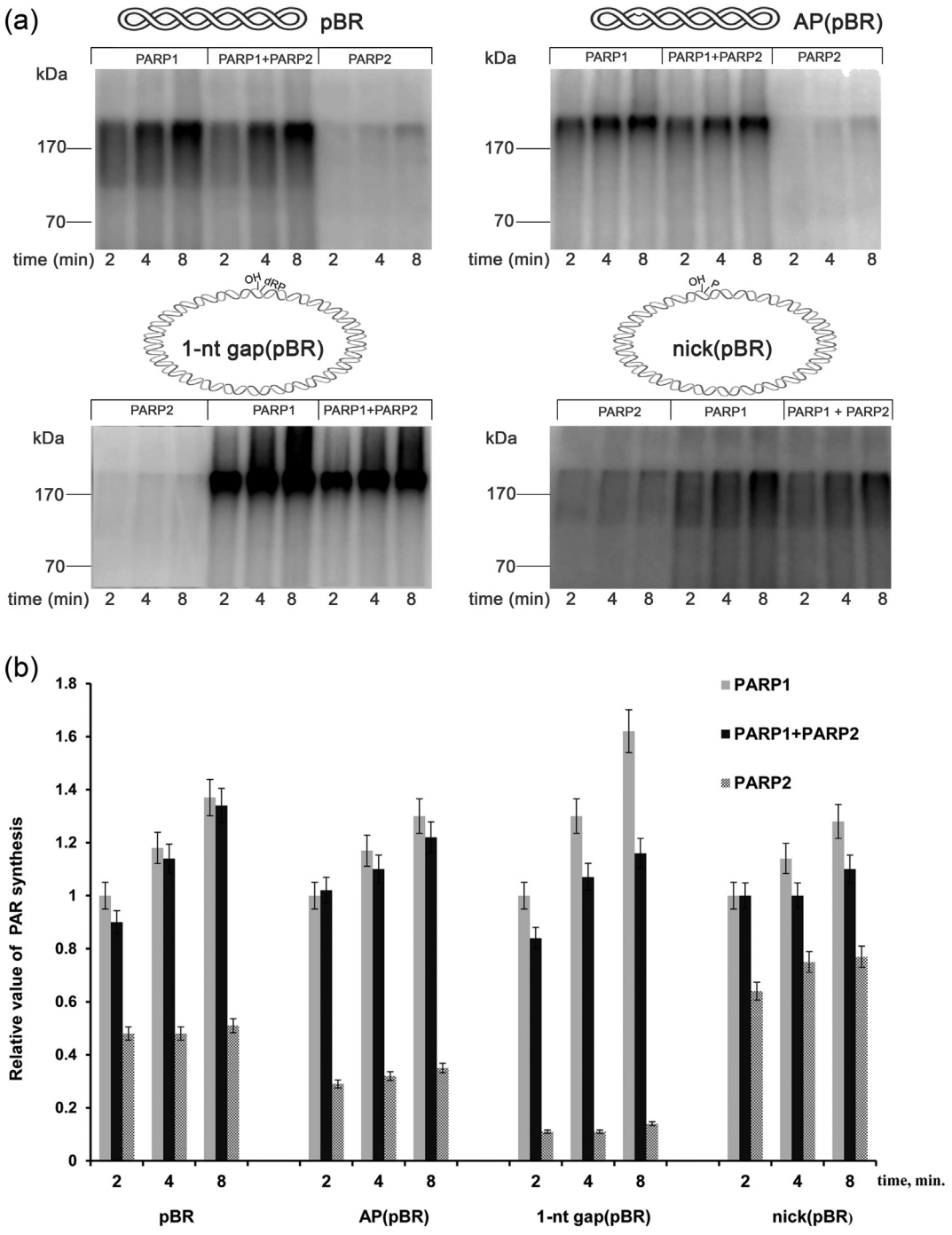

Fig. 8. PARP2 negatively regulates PARP1 activity. (a) The time-course of activity of PARP1 alone, PARP2 alone, and PARP1 mixed with PARP2 in the presence of different plasmid DNAs and [^{32}P]NAD$^+$ analyzed by SDS-PAGE. (b) The diagram presents quantification of [^{32}P]-labeled PAR. The data denote mean values and standard deviations from three independent experiments including the experiment in (a). The relative productivity of PAR synthesis measured in the presence of pBR, AP(pBR), 1-nt gap(pBR), or nick(pBR) was normalized to the productivity of PAR synthesis catalyzed by PARP1 alone for 2 min with each DNA substrate.

presence of NAD$^+$ and the formation of PAR polymers was detected by AFM (Fig. 7a). PARylation of PARPs was observed for all DNA plasmids, but we did not observe specific features of shape of PAR polymers formed in the presence of AP site, 1-nt gap, or nick (e.g., PARP1 PARylation, see Fig. 7b). PARylated proteins looked like branched "star"-like structures of different size for all DNAs used [41].

Therefore, the DNA lesions affected the mode of PAR synthesis differently in the case of PARP1 and PARP2 (Fig. 6). In the case of PARP1, a marked increase in the catalytic activity was observed only for a plasmid bearing a single 1-nt gap, but production of long PAR polymers was only slightly more effective relative to other plasmid DNAs. For PARP2, single DNA damage (1-nt gap or nick) increased the enzymatic activity and the amount of long PAR polymers. These results are consistent with our previous finding that the size of PAR produced by PARP2 depends on the initial affinity of this protein for DNA breaks [41]. On the other hand, the type of DNA damage can influence PARP1 catalytic activity, but the PAR chain length distribution is affected only weakly.

PARP2 competes with PARP1 for the binding to BER intermediates and influences PAR synthesis

Although numerous studies have proved the dependence of BER and SSBR on PARP1, the participation of PARP2 and PAR formation in the repair process is still debated [10,36]. It has been demonstrated before that PARP2 is less effective in PAR synthesis than PARP1 both *in vitro* and *in vivo* [20,35]. It appears that PARP2-dependent PAR synthesis has a smaller influence than PARP1 on the regulation of the BER process [11,13,54,55]. Nevertheless, PARP2 can regulate BER and SSBR not only directly through interaction with BER enzymes and DNA intermediates but also indirectly via regulation of PARP1 activity [12,20]. For example, PARP2 can compete with PARP1 for the binding to DNA repair intermediates, thereby preventing PARP1 activation. The ability of PARP2 to suppress PARP1 activity has been detected by using of short DNA duplexes mimicking DNA intermediates of different DNA damage repair pathways [20]. We next tested whether PARP2 impairs the activity of PARP1 when DNA substrates were represented by plasmid DNAs containing single-strand DNA damage (AP site, 1-nt gap, or nick) (Fig. 1b). To this end, we analyzed total PAR synthesis, when both proteins were present in the reaction at equimolar amounts (Fig. 8). The relative PAR synthesis activity of PARP1 and PARP2, and of the mixture of PARP1 and PARP2 was analyzed in a time-dependent manner as fold activation above or below the levels of PARP1-catalyzed PAR synthesis after a 2-min reaction for each DNA substrate (Fig. 8b). We first estimated PAR synthesis catalyzed by PARP2 relative to PARP1 (Fig. 8b). Indeed, we observed a lower activity of PARP2 compared to PARP1; however, the difference in the level of their autoPARylation was strongly dependent on the type of DNA substrates. The quantitative analysis shows that PARP2 was less efficient in PAR production than PARP1 (Fig. 8b). The level of PARP2 PARylation in the presence of nicked, intact, AP site, or 1-nt gapped plasmid DNA turned out to be approximately 1.7-, 2.7-, 3.7-, and 11.4-fold lower in comparison with the PARP1 reactions. When the PAR synthesis was analyzed in the equimolar mixture of the two proteins, the productivity of PAR synthesis for PARP1 was almost unaffected by the presence of PARP2 when intact DNA plasmid (pBR) or AP(pBR) was used as a substrate (Fig. 8b). For plasmid DNAs bearing a 1-nt gap or nick, the presence of PARP2 led to a decrease of PAR synthesis in comparison with the reaction catalyzed by PARP1 alone (Fig. 8b). When PARP2 was added together with PARP1, the productivity of PAR formation decreased by 30% and 15% for 1-nt gap(pBR) and nick(pBR) substrates, respectively (Fig. 8b).

Altogether, these results suggest that PARP2's influence on the productivity of PAR synthesis was more pronounced when DNAs bearing 1-nt gap or nick were used for PARP activation. Consequently, in the context of PARP1 activation by SSBs formed during BER, PARP2 can efficiently recognize and bind to the repair intermediates and affects PAR synthesis by suppressing and/or changing the kinetics of this reaction.

Discussion

BER and SSBR are the main pathways for the removal of damaged bases and processing of AP sites and SSBs in mammalian cells [5]. The repair process can be modulated by accessory factors, among them PARP1 and PARP2 [9,12]. Both PARPs are known to function in BER and SSBR by interacting with repair enzymes and BER DNA intermediates or by promoting the synthesis of PAR at the site of DNA damage [13,36,55]. Although numerous studies support the importance of PARP1 for BER regulation, the function of PARP2 in this repair is not fully understood yet, but PARP2 along with PARP1 seems to contribute to the repair process [10,12,15]. On the one hand, PARP2 has been proposed to play an auxiliary role in BER, by functioning as a “backup” polymerase when the function of PARP1 is impaired [12,15]. On the other hand, these PARPs may perform different functions in DNA repair [54,56,57]. The ability of PARP2 to influence the enzymatic activity of PARP1 gave rise to the assumption that PARP2 may be effective at regulation of PARP1 activation [12,20,58].

Previously, our comparative analysis of PARP1 and PARP2 interactions with BER intermediates has been restricted by the use of short DNA duplexes [20]. Using long DNA and AFM single-molecule visualization enabled us to examine

PARP1 and PARP2 activation by different types of single-strand DNA damage. The research presented here extends our previous works and provides further insight into the recognition of DNA repair intermediates followed by PAR synthesis catalyzed by these polymerases. The general aim was to find possible differences between the interactions of PARP1 and PARP2 with the types of single-strand DNA damage that mimic BER intermediates, namely, AP site, 1-nt gap, and nick. Accordingly, this investigation was focused on the quantitative characterization of PARP1 and PARP2 binding to different DNA damage sites and on the comparison of catalytic activities of PARPs on these DNA structures formed during BER. Our experiments indicate that the affinity of PARP1 for an AP site and 1-nt gap is higher than that of PARP2; meanwhile, both proteins bind to a nick with similar affinity. This finding suggests that PARP1 participates in early steps of BER, whereas both PARPs efficiently interact with a nick and may contribute to the regulation of the final repair stage: ligation performed by the DNA ligase III–XRCC1 complex. It is noteworthy that PARP1 has a preference for binding to a 1-nt gap over an AP site or nick, but PARP2 shows binding preference for a nick over a 1-nt gap or AP site, thus pointing to damage-specific binding to DNA intermediates in BER.

Our data also reveal that PARP1 binds to undamaged DNA, an AP site, or a 1-nt gap mainly as a monomer, but the interaction with a nick takes place in both monomeric and dimeric forms. Similar to PARP1, PARP2 was found to bind to undamaged DNA and AP sites as a monomer; however, PARP2 dimerizes on a 1-nt gap or nick site. Furthermore, autoPARylation of PARP1 appears to depend on the oligomerization state (monomer *versus* dimer): the binding of PARP1 in the monomeric form to a 1-nt gap leads to strong activation of PARP1, whereas dimer formation at the nick site leads to less effective autoPARylation (Figs. 5a and 6a). In the case of PARP2, its dimerization at SSBs (a nick or 1-nt gap) probably causes more effective automodification (Figs. 5c and 6b). Consequently, the monomer-to-dimer transition can contribute to the regulation of enzymatic activity of PARPs. Besides, it should be noted that in contrast to PARP1, the efficiency of autoPARylation of PARP2 and polymer chain formation is greatly affected by PARP2's initial affinity for the single-strand break DNA damage sites (Table 1 and Fig. 6c).

We also demonstrate that PARP2 can modulate the PAR synthesis catalyzed by PARP1, and this effect apparently correlates with the initial affinity of PARP2 for DNA damage. Total PAR synthesis in the presence of intact or AP site–containing DNA was affected to a lesser extent by the addition of PARP2 to PARP1, implying that these proteins compete with each other or form heterodimers at SSBs, such as a 1-nt gap or nick [12,20]. Taking into account the importance of PARP1 activation and PAR formation for modulation of DNA repair [11,13,29,55,57], one could expect indirect implication of PARP2 in BER via regulation of PARP1-catalyzed PAR synthesis. In these cases, the activity of PARP1 can be suppressed by the binding of PARP2 to the DNA damage site or by formation of a functional heterodimer that has a lower PAR synthesis activity in comparison with the PARP1 homodimer. In support of this hypothesis, PARP2 has been reported to be effective at inhibiting PAR synthesis catalyzed by PARP1 in the presence of various DNA substrates [20]. Moreover, cell experiments show that PARP2 depletion increases PAR formation in thymocytes and B cells [59,60].

Therefore, the functions of PARP1 and PARP2 in BER after SSB formation may overlap, providing evidence for the participation of PARP2 in the regulation of PARP1 activity through competition for DNA binding and/or changes in the kinetics of PAR synthesis. The PARP1-driven synthesis of PAR and the kinetics of PAR synthesis have important functions in the regulation of BER and SSBR *in vivo* and *in vitro* [15,54,55]. Therefore, PARP2 in addition to direct interaction with BER DNA intermediates may indirectly influence BER via regulation of PAR synthesis by PARP1 after SSB formation during BER.

Materials and Methods

Materials

The pET32a-hPARP-1-His and pXC53-hAPE1 plasmids and the mPARP-2 recombinant baculovirus were kindly provided by Dr. M. Satoh (Laval University, Canada), Dr. S. H. Wilson (NIEHS, NIH, USA), and by Dr. Valerie Schreiber (Université de Strasbourg, IREBS, Illkirch, France), respectively. The human recombinant proteins PARP1 and APE1 were overexpressed in *Escherichia coli* and purified as described previously [16,19]. Murine PARP2 was expressed in insect cells and purified according to protocol described by Amé *et al*. [61]. Yeast nicotinamide mononucleotide adenylyltransferase (NMNAT) was kindly provided by Dr. Stanislav I. Shramm (IMG RAS, Moscow, Russia). Recombinant *E. coli* uracil DNA glycosylase (UDG) was acquired from Biosan, whereas plasmid pBR322 and AseI and NotI restriction enzymes as well as Nb.BsmI (a nicking endonuclease) were from New England BioLabs. Restriction enzymes BglII and BamHI, Taq DNA polymerase, and T4 DNA ligase were purchased from Thermo Scientific-Fermentas, and DNA polymerase I (Large [Klenow] fragment) was from

Invitrogen. AfeI and SmaI restriction enzymes and SE buffer were bought from SibEnzyme, whereas radioactive [^{32}P]ATP and α[^{32}P]dCTP were produced in the Laboratory of Biotechnology (ICBFM SB RAS). Synthetic oligonucleotides were produced in the Laboratory of Medicinal Chemistry (ICBFM SB RAS). Chemicals [$MgCl_2$, putrescine, dNTPs, putrescine, β-NAD^+, and 5(6)-carboxyfluorescein *N*-hydroxysuccinimide ester (FSE)] were purchased from Sigma-Aldrich.

Preparation of long DNA substrates and plasmid DNA

The DNA duplex (0.5 μM) 31mer with uracil was obtained by hybridization of an oligonucleotide (5′P-gatcctctagagtcgac**U**ctgcaggcatgcg-3′) with the complementary oligonucleotide in a 1:1 ratio. Oligonucleotide mixtures were incubated for 3 min at 95 °C and then slowly cooled to room temperature. The 1400-bp DNA fragment was prepared after insertion of the 31mer DNA duplex containing uracil at a defined position and of 4-nucleotide 5′ overhangs into the mutant pEGFP-N1 plasmid (without a BamHI site) according to a protocol described by Enoiu *et al.* [62] with some modifications. Briefly, to prepare a sticky-ended linearized plasmid, 10 μg of a mutant pEGFP-N1-bis plasmid was completely digested with 0.5 U/μl BglII in 1× FastDigest buffer at 37 °C for 2 h, as determined by 0.8% agarose gel electrophoresis of an aliquot (Fig. S5). After that, the linearized plasmid was deproteinized with phenol and chloroform, precipitated with ethanol, and resuspended in TE buffer. The linearized plasmid (0.02 pmol/μl) containing 4-nucleotide 5′ overhangs was ligated to the complimentary 5′ phosphorylated ends of a 31mer DNA duplex (0.02 pmol/μl) using 1.5 U/μl T4 DNA ligase at 4 °C overnight in FastDigest buffer (Fermentas) and 0.5 mM ATP in the presence of 0.06 U/μl BamHI and 0.06 U/μl BglII. The ligated products were deproteinized by extraction with phenol–chloroform followed by ethanol precipitation. The precipitated DNA pellets were resuspended and digested with 0.3 U/μl AseI and NotI in 1× NE Buffer 3 at 37 °C for 3 h. Next, the sticky ends of the DNA fragments were filled using 0.075–0.225 U/μl DNA polymerase I, Large (Klenow) fragment in the presence of four dNTPs to a final concentration of 250 μM each at 37 °C for 3 h. The obtained DNA fragments were purified in 1.5% agarose, and bands corresponding to 1400-bp DNA fragments were excised and purified with the Gel Extraction Kit (Fermentas). The yield of the U-containing 1421-bp DNA fragment [U(1400-bp)] was 5% of the starting plasmid.

To verify the presence of a site-specific U at position 622 bp from one end in the purified fragment, 0.9 nM U(1400-bp) DNA was incubated with 1 U/μl UDG for 15 min at 37 °C in a buffer consisting of 20 mM Tris–HCl (pH 8.0), 1 mM DTT, 20 mM NaCl, and 1 mM EDTA and then incubated with 20 nM APE1 and 300 nM pol β in the presence of 5 mM $MgCl_2$ and 20 μCi α[^{32}P]dCTP for 30 min at 37 °C, followed by heat inactivation for 20 min at 65 °C. The resulting products were subjected to restriction digestion with 0.5 U/μl AfeI and 0.5 U/μl SmaI in SE buffer for 1 h at 37 °C (Fig. S6). The reactions were stopped by the addition of a 2-fold volume of a solution consisting of 90% of formamide, 10 mM EDTA, 0.1% of bromophenol blue, and 0.1% of xylene cyanol, then the mixtures were heated at 90 °C for 3 min, and the products were separated by denaturing electrophoresis in a 10% polyacrylamide gel. The gels were dried and subjected to phosphorimaging for quantification using Molecular Imager (Bio-Rad) and software (Quantity One).

To prepare the 1421-bp DNA fragment containing a single AP site [AP(1400-bp)], the 2.8 nM DNA fragment was incubated with 12 nM UDG in a buffer consisting of 20 mM Tris–HCl (pH 8).0, 20 mM NaCl, 1 mM DTT, and 1 mM EDTA for 20 min at 37 °C. To prepare the 1421-bp DNA fragment containing an SSB with 3′-OH and a 5′-dRP 1-nt gap [1-nt gap(1400-bp)], the 2.8 nM DNA fragment with the AP site was treated with 25 nM APE1 in the presence of 5 mM $MgCl_2$ for 20 min at 37 °C. The 1200-bp DNA fragment containing an SSB with 3′-OH and a 5′-P nick nick(1200-bp) was prepared by means of the Nb.BsmI nicking endonuclease as described elsewhere [41].

The pBR plasmid containing up to two AP sites per DNA circle was prepared by heat and acid treatment [63]. Briefly, plasmid DNA (0.25 mg/ml) was incubated in a buffer consisting of 20 mM sodium citrate (pH 5.0) and 200 mM NaCl at 70 °C for 30 min. The reactions were stopped by the addition of 1 M Tris–HCl (pH 8.0), rapidly chilled on ice, and subjected to the analysis. To prepare the pBR plasmid containing up to two SSBs with 3′-OH and 5′-dRP [1-nt gap (pBR)], the AP site-containing pBR plasmid (29 nM) was incubated with 20 nM APE1 in 1× NE Buffer 1 for 1 h at 37 °C, followed by heat inactivation for 10 min at 65 °C. The amounts of supercoiled and circular forms of DNA were estimated by 0.8% agarose gel electrophoresis (Fig. S2) [63]. Agarose gel electrophoresis showed that this treatment introduces approximately one AP site (1-nt gap) per DNA molecule within 30 min (Fig. S2b and c). DNA concentrations were determined by measuring absorbance at 260 nm. Due to the labile nature of the UDG- or APE1-treated DNA, all the DNA substrates were prepared just before AFM or biochemical experiments. Nicked pBR were obtained by incubating pBR322 with Nb.Bsm1 nicking endonuclease according to the recommended protocol.

AFM

Protein complexes for AFM analysis were formed in reaction mixtures (20 µl) containing binding buffer [12.5 mM Hepes (pH 8.0), 12.5 mM KCl, and 1 mM DTT], 2 nM PARP1 or 3.6 nM PARP2 and 0.8–1.0 nM DNA substrate. For experiments with a mixture of DNA substrates, 3.5 nM PARP1 or 7 nM PARP2 was incubated with an equimolar amount of 1200-bp or nick(1200-bp) and 1-nt gap(1400-bp) in binding buffer. According to our previous studies, putrescine (Pu^{2+}) was selected as counterion for PARP1(2), protein–DNA complex, and PARylated PARPs adsorption on mica surface [41]. The reactions were incubated on ice for 1–5 min followed by the addition of putrescine (Pu^{2+}) to a final concentration of 5 mM. After that, a 10-µl droplet was deposited on the surface of freshly cleaved mica at room temperature for 30-s incubation and was dried for AFM imaging. For experiments with auto-PARylation of PARP1, 35 nM PARP1 was incubated with 3.5 nM nicked pBR, supercoiled pBR, AP-pBR, or 1-nt gap-pBR in the AFM deposition buffer in the presence of 100 µM NAD^+ and 10 mM $MgCl_2$ at 37 °C for 15–120 min. Next, the samples were diluted 10-fold in AFM deposition buffer containing 5 mM Pu^{2+} and immediately deposited on mica. AFM images were captured in air on a Nanoscope V Multimode 8 (Bruker, Santa-Barbara, CA, USA) in PeakForce Tapping (PFT) mode with Scanasyst-Air probes (Bruker). In this experiment, continuous force–distance curves were recorded at 2048 × 2048 pixels at a line rate of 1.5 Hz, and the tip was oscillated in the vertical direction with an amplitude of 100–300 nm and at low frequency (1–2 kHz).

AFM data analysis

The "section" tool in the Nanoscope Analysis software (version 1.70) was employed to determine the molecular dimensions of the protein particles. Cross-sections of PARP1(2) alone or interacting with DNA were made, and the height (h) and diameter (r) at half-maximal height of each single particle were measured (Fig. S3a). The molecular volume of the protein particles was determined according to the following equation [64]:

$$V = \frac{\pi h}{6}\left(3r^2 + h^2\right)$$

The volumes were calculated from two scanned areas (3 × 3 µm) and two independent samples. Significance of differences in volume measurements was determined by the t test. Measurements of parameters h and r were also performed on naked DNA to assess the influence of the tip and the scan parameters on the volume measurements (Fig. S3c). The DNA contour length and PARP1(2)-binding position on DNA were analyzed in the ImageJ software as presented in Fig. S1d–f and described elsewhere [41]. The length of the DNA contour was manually traced in AFM images. In the case of DNA–protein complexes, the contour length was manually traced as the shortest possible DNA path through the bound protein.

The AFM site-specific binding affinity (K_D) values of PARP1(2) for the AP site, 1-nt gap, or nick were calculated directly by estimating the number of specific and nonspecific complexes and fractional occupancy rates of proteins bound to specific DNA sites (Table S1) as described previously [65]. Specific sites correspond to AP, 1-nt gap, or nick sites, whereas nonspecific sites correspond to all other DNA sites, including undamaged DNA and DNA ends. PARP1(2) interacts with specific site when it is localized between 194 and 224 nm from one 1400-bp DNA end. For nick site, PARP should be localized between 199 and 229 nm from nick (1200-bp) DNA end (Figs. 1a and S1d–f).

Fluorescence titration and calculation of apparent binding constants of complexes of PARP1 or PARP2 with plasmid DNA substrates containing a single DNA damage site

Fluorescence measurements were performed on a POLARstar Optima multidetection microplate reader (BMG Labtech, Offenburg, Germany) in a 96-well assay "V" bottom black plate (Axigen), and thus, one well contained one titration point. As a substrate, we chose fluorescein-labeled PARP1(2) (Flu-PARP1 and -2). These proteins were labeled with FSE as described previously [41]. The concentrations of Flu-PARP1(2) conjugates and labeling efficiency were determined according to the manufacturer's protocol (Thermo Scientific) via the following extinction coefficients: ε_{280} = 120,000 M^{-1} cm^{-1} for PARP1, ε_{280} = 70415 M^{-1} cm^{-1} for PARP2, and ε_{280} = 23400 cm^{-1} M^{-1} and ε_{495} = 60000 M^{-1} cm^{-1} for fluorescein. The degree of labeling was determined: 96% for PARP1 and 90% for PARP2. Titration was carried out by adding various amounts of plasmid DNA (0.1–20.0 nM) to a fixed concentration (5–10 nM) of Flu-PARP1 or Flu-PARP2 in a buffer consisting of 50 mM Hepes–KOH (pH 8.0), 50 mM NaCl, and 1 mM DTT. The excitation wavelength was set to 485 nm, and emission wavelength was set to 520 nm. All the reaction mixtures were prepared at room temperature. The plate was incubated at 28 °C in the microplate reader. Each experiment was repeated at least three times.

An SDS-PAGE–based radioactive assay of PARP1 and PARP2 autoPARylation

[^{32}P]NAD labeled on the adenylate phosphate was synthesized as described earlier [66] with some modifications. Briefly, the reaction mixture (100 μl) containing 2 mM β-nicotinamide mononucleotide, 1 mM ATP, 0.25 mCi of [α-^{32}P]ATP (1000 Ci/mmol), 1.5 mg/ml NMNAT, 25 mM Tris–HCl (pH 7.5), and 20 mM $MgCl_2$ was incubated for 1 h at 37 °C. The enzyme was denatured for 10 min at 65 °C, and precipitated protein was removed by centrifugation.

The poly(ADP-ribosyl)ation assay was performed in the reaction mixtures (50 μl) consisting of 50 mM Hepes–KOH (pH 8.0), 50 mM NaCl, 1 mM DTT, 5 mM $MgCl_2$, 3 nM plasmid DNA, 100–10 μM NAD^+ supplemented with 8 μCi of [^{32}P]NAD^+, and 20 nM PARP1 or PARP2. The reactions were initiated by the addition of NAD^+. The reaction mixtures were incubated at 37 °C for 2–45 min, and the assay was stopped by adding SDS sample buffer and heating for 5 min at 90 °C. The reaction mixtures were analyzed by 10% SDS-PAGE (Fig. S4a and b). The gels were dried and subjected to phosphorimaging for quantification using Molecular Imager (Bio-Rad) and software (Quantity One).

The chemical release and analysis of protein-free poly(ADP-ribose) polymers

To analyze the length of PAR synthesized by PARP1 or PARP2, the reactions were carried out in mixtures (80–120 μl) consisting of 50 mM Hepes-KOH pH 8.0, 50 mM NaCl, 1 mM DTT, 5 mM $MgCl_2$, 3 nM plasmid DNA, 50 mg/ml BSA, 20 nM PARP2 or PARP1, and 10 μM NAD^+ supplemented with 8 μCi of [^{32}P]NAD^+. The reactions were initiated by the addition of NAD^+ followed by incubation at 37 °C for 15 min for PARP1 and 45 min for PARP2. The reactions were stopped by the addition of an equal volume of 20% trichloroacetic acid and were processed as described earlier [53]. The chemical release of PAR chains was performed in 0.1 N NaOH, 20 mM EDTA at 60 °C for 2 h according to Ref. [53], after which the samples were neutralized with 0.1 N HCl, dried in a vacuum concentrator, resuspended in an aqueous solution (50% of urea, 25 mM NaCl, and 4 mM EDTA), and analyzed in a modified DNA sequencing gel [67]. The gels were dried and subjected to phosphorimaging using Molecular Imager (Bio-Rad) and software (Quantity One) for quantification of PAR polymer production (Fig. S4c). The size distribution of PAR polymers was determined as the average content (%) of a short-, medium-, or long-polymer fraction relative to the total amount of polymers produced during the reaction.

Acknowledgments

This work was supported by the Russian Scientific Foundation (projects No. 17-74-20075 for M.V.S. and M.M.K. and No 19-14-00107 for O.I.L.), Russian State-funded budget project of ICBFM SB RAS (No. AAAA-A17-117020210022-4), INSERM, and the Genopole Evry. The English language was corrected and certified by shevchuk-editing.com.

Appendix A. Supplementary data

Supplementary data to this article can be found online at https://doi.org/10.1016/j.jmb.2019.05.028.

Received 29 December 2018;
Received in revised form 15 April 2019;
Available online 23 May 2019

Keywords:
poly(ADP-ribose) polymerase 1;
poly(ADP-ribose) polymerase 2;
base excision repair;
single-molecule analysis;
atomic force microscopy

†These authors contributed equally to this work.

Abbreviations used:
1-nt gap, one-nucleotide gap; AP, apurinic/apyrimidinic; APE1, apurinic/apyrimidinic endonuclease 1; BER, base excision repair; dRP, deoxyribose phosphate; P, phosphate; PAGE, polyacrylamide gel electrophoresis; PAR, poly(ADP-ribose); PARP, poly(ADP-ribose) polymerase; SSB, single-strand break; SSBR, single-strand break repair.

References

[1] T. Lindahl, Instability and decay of the primary structure of DNA, Nature 362 (1993) 709–715.
[2] A. Torgovnick, B. Schumacher, DNA repair mechanisms in cancer development and therapy, Front. Genet. 6 (2015) 157.
[3] R.N. Trivedi, K.H. Almeida, J.L. Fornsaglio, S. Schamus, R. W. Sobol, The role of base excision repair in the sensitivity and resistance to temozolomide-mediated cell death, Cancer Res. 65 (2005) 6394–6400.
[4] A. Ciccia, S.J. Elledge, The DNA damage response: making it safe to play with knives, Mol. Cell. 40 (2010) 179–204.
[5] T. Lindahl, D.E. Barnes, Repair of endogenous DNA damage, Cold Spring Harbor Symposia on Quantitative Biology, vol. 65, Cold Spring Harbor Laboratory Press 2000, pp. 127–134.

[6] H.E. Krokan, M. Bjørås, Base excision repair, Cold Spring Harb. Perspect. Biol. 5 (2013), a012583.
[7] G.L. Dianov, U. Hübscher, Mammalian base excision repair: the forgotten archangel, Nucleic Acids Res. 41 (2013) 3483–3490.
[8] T. Lindahl, M.S. Satoh, G.G. Poirier, A. Klungland, Post-translational modification of poly (ADP-ribose) polymerase induced by DNA strand breaks, Trends Biochem. Sci. 20 (1995) 405–411.
[9] F. Dantzer, V. Schreiber, C. Niedergang, C. Trucco, E. Flatter, G. De La Rubia, J. Oliver, V. Rolli, J. Ménissier-de Murcia, G. de Murcia, Involvement of poly (ADP-ribose) polymerase in base excision repair, Biochimie 81 (1999) 69–75.
[10] J. Yélamos, V. Schreiber, F. Dantzer, Toward specific functions of poly (ADP-ribose) polymerase-2, Trends Mol. Med. 14 (2008) 169–178.
[11] D. D'Amours, S. Desnoyers, I. D'Silva, G.G. Poirier, Poly (ADP-ribosyl)ation reactions in the regulation of nuclear functions, Biochem. J. 342 (1999) 249–268.
[12] V. Schreiber, J.C. Amé, P. Dollé, I. Schultz, B. Rinaldi, V. Fraulob, J. Menissier-de Murcia, G. de Murcia, Poly (ADP-ribose) polymerase-2 (PARP-2) is required for efficient base excision DNA repair in association with PARP-1 and XRCC1, J. Biol. Chem. 277 (2002) 23028–23036.
[13] V. Schreiber, F. Dantzer, J.C. Ame, G. De Murcia, Poly (ADP-ribose): novel functions for an old molecule, Nat. Rev. Mol. Cell Biol. 7 (2006) 517–528.
[14] J.M. de Murcia, M. Ricoul, L. Tartier, C. Niedergang, A. Huber, F. Dantzer, V. Schreiber, J.C. Amé, A. Dierich, M. LeMeur, L. Sabatier, P. Chambon, G. de Murcia, Functional interaction between PARP-1 and PARP-2 in chromosome stability and embryonic development in mouse, EMBO J. 22 (2003) 2255–2263.
[15] H. Hanzlikova, W. Gittens, K. Krejcikova, Z. Zeng, K.W. Caldecott, Overlapping roles for PARP1 and PARP2 in the recruitment of endogenous XRCC1 and PNKP into oxidized chromatin, Nucleic Acids Res. 45 (2016) 2546–2557.
[16] N.A. Moor, I.A. Vasil'eva, R.O. Anarbaev, A.A. Antson, O.I. Lavrik, Quantitative characterization of protein–protein complexes involved in base excision DNA repair, Nucleic Acids Res. 43 (2015) 6009–6022.
[17] R.J. Sanderson, T. Lindahl, Down-regulation of DNA repair synthesis at DNA single-strand interruptions in poly (ADP-ribose) polymerase-1 deficient murine cell extracts, DNA Repair 1 (2002) 547–558.
[18] O.I. Lavrik, R. Prasad, R.W. Sobol, J.K. Horton, E.J. Ackerman, S.H. Wilson, Photoaffinity labeling of mouse fibroblast enzymes by a base excision repair intermediate, J. Biol. Chem. 276 (2001) 25541–25548.
[19] M. Sukhanova, S. Khodyreva, O. Lavrik, Poly (ADP-ribose) polymerase 1 regulates activity of DNA polymerase β in long patch base excision repair, Mutat. Res. Fundam. Mol. Mech. Mutagen. 685 (2010) 80–89.
[20] M.M. Kutuzov, S.N. Khodyreva, J.C. Amé, E.S. Ilina, M.V. Sukhanova, V. Schreiber, O.I. Lavrik, Interaction of PARP-2 with DNA structures mimicking DNA repair intermediates and consequences on activity of base excision repair proteins, Biochimie 95 (2013) 1208–1215.
[21] M.M. Kutuzov, S.N. Khodyreva, E.S. Ilina, M.V. Sukhanova, J.C. Ame, O.I. Lavrik, Interaction of PARP-2 with AP site containing DNA, Biochimie 112 (2015) 10–19.
[22] N.N. Hooten, K. Kompaniez, J. Barnes, A. Lohani, M.K. Evans, Poly (ADP-ribose) polymerase 1 (PARP-1) binds to 8-oxoguanine-DNA glycosylase (OGG1), J. Biol. Chem. 286 (2011) 44679–44690.
[23] I. Frouin, G. Maga, M. Denegri, F. Riva, M. Savio, S. Spadari, E. Prosperi, A.I. Scovassi, Human proliferating cell nuclear antigen, poly (ADP-ribose) polymerase-1, and p21waf1/cip1 a dynamic exchange of partners, J. Biol. Chem. 278 (2003) 39265–39268.
[24] B.C. Woodhouse, I.I. Dianova, J.L. Parsons, G.L. Dianov, Poly (ADP-ribose) polymerase-1 modulates DNA repair capacity and prevents formation of DNA double strand breaks, DNA Repair 7 (2008) 932–940.
[25] J.B. Tang, E.M. Goellner, X.H. Wang, R.N. Trivedi, C.M. St Croix, E. Jelezcova, D. Svilar, A.R. Brown, R.W. Sobol, Bioenergetic metabolites regulate base excision repair-dependent cell death in response to DNA damage, Mol. Cancer Res. 8 (2010) 67–79.
[26] C. Cistulli, O.I. Lavrik, R. Prasad, E. Hou, S.H. Wilson, AP endonuclease and poly (ADP-ribose) polymerase-1 interact with the same base excision repair intermediate, DNA Repair 3 (2004) 581–591.
[27] N.A. Lebedeva, N.I. Rechkunova, S.N. Khodyreva, A. Favre, O.I. Lavrik, Photoaffinity labeling of proteins in bovine testis nuclear extract, Biochem. Biophys. Res. Commun. 297 (2002) 714–721.
[28] S.N. Khodyreva, R. Prasad, E.S. Ilina, M.V. Sukhanova, M. M. Kutuzov, Y. Liu, E.W. Hou, S.H. Wilson, O.I. Lavrik, Apurinic/apyrimidinic (AP) site recognition by the 5′-dRP/AP lyase in poly (ADP-ribose) polymerase-1 (PARP-1), Proc. Natl. Acad. Sci. U. S. A. 107 (2010) 22090–22095.
[29] M.F. Langelier, A.A. Riccio, J.M. Pascal, PARP-2 and PARP-3 are selectively activated by 5′ phosphorylated DNA breaks through an allosteric regulatory mechanism shared with PARP-1. Nucleic, Acids Res. 42 (2014) 7762–7775.
[30] E. Obaji, T. Haikarainen, L. Lehtiö, Characterization of the DNA dependent activation of human ARTD2/PARP2, Sci. Rep. 6 (2016), 34487.
[31] C. Liu, A. Vyas, M.A. Kassab, A.K. Singh, X. Yu, The role of poly ADP-ribosylation in the first wave of DNA damage response, Nucleic Acids Res. 45 (2017) 8129–8141.
[32] H. Wei, X. Yu, Functions of PARylation in DNA damage repair pathways, Genom. Proteom. Bioinf. 14 (2016) 131–139.
[33] W.M. Shieh, J.C. Amé, M.V. Wilson, Z.Q. Wang, D.W. Koh, M.K. Jacobson, E.L. Jacobson, Poly (ADP-ribose) polymerase null mouse cells synthesize ADP-ribose polymers, J. Biol. Chem. 273 (1998) 30069–30072.
[34] M. Masson, C. Niedergang, V. Schreiber, S. Muller, J. Menissier-de Murcia, G. de Murcia, XRCC1 is specifically associated with poly (ADP-ribose) polymerase and negatively regulates its activity following DNA damage, Mol. Cell. Biol. 18 (1998) 3563–3571.
[35] J.C. Amé, V. Rolli, V. Schreiber, C. Niedergang, F. Apiou, P. Decker, S. Muller, T. Hoger, J. Menissier-de Murcia, G. de Murcia, PARP-2, a novel mammalian DNA damage-dependent poly (ADP-ribose) polymerase, J. Biol. Chem. 274 (1999) 17860–17868.
[36] M.M. Kutuzov, S.N. Khodyreva, V. Schreiber, O.I. Lavrik, Role of PARP2 in DNA repair, Mol. Biol. (Moscow) 48 (2014) 485–495.
[37] A.A. Riccio, G. Cingolani, J.M. Pascal, PARP-2 domain requirements for DNA damage-dependent activation and localization to sites of DNA damage, Nucleic Acids Res. 44 (2015) 1691–1702.
[38] I. D'Silva, J.D. Pelletier, J. Lagueux, D. D'Amours, M.A. Chaudhry, M. Weinfeld, S.P. Lees-Miller, G.G. Poirier,

Relative affinities of poly (ADP-ribose) polymerase and DNA-dependent protein kinase for DNA strand interruptions, Biochim. Biophys. Acta Protein Struct. Mol. Enzymol. 1430 (1999) 119–126.
[39] I. Lonskaya, V.N. Potaman, L.S. Shlyakhtenko, E.A. Oussatcheva, Y.L. Lyubchenko, V.A. Soldatenkov, Regulation of poly (ADP-ribose) polymerase-1 by DNA structure-specific binding, J. Biol. Chem. 280 (2005) 17076–17083.
[40] M.H. Chassé, U.M. Muthurajan, N.J. Clark, M.A. Kramer, S. Chakravarthy, T. Irving, K. Luger, Biochemical and biophysical methods for analysis of poly (ADP-ribose) polymerase 1 and its interactions with chromatin, Methods Mol. Biol. 1608 (2017) 231–253.
[41] M.V. Sukhanova, S. Abrakhi, V. Joshi, D. Pastre, M.M. Kutuzov, R.O. Anarbaev, P.A. Curmi, L. Hamon, O.I. Lavrik, Single molecule detection of PARP1 and PARP2 interaction with DNA strand breaks and their poly (ADP-ribosyl)ation using high-resolution AFM imaging, Nucleic Acids Res. 44 (2016) e60.
[42] C.N. Buechner, I. Tessmer, DNA substrate preparation for atomic force microscopy studies of protein–DNA interactions, J. Mol. Recognit. 26 (2013) 605–617.
[43] H. Mendoza-Alvarez, R. Alvarez-Gonzalez, Poly (ADP-ribose) polymerase is a catalytic dimer and the automodification reaction is intermolecular, J. Biol. Chem. 268 (1993) 22575–22580.
[44] E. Pion, G.M. Ullmann, J.C. Amé, D. Gérard, G. de Murcia, E. Bombarda, DNA-induced dimerization of poly (ADP-ribose) polymerase-1 triggers its activation, Biochemistry 44 (2005) 14670–14681.
[45] A.A. Ali, G. Timinszky, R. Arribas-Bosacoma, M. Kozlowski, P.O. Hassa, M. Hassler, A.G. Ladurner, L.H. Pearl, A.W. Oliver, The zinc-finger domains of PARP1 cooperate to recognize DNA strand breaks, Nat. Struct. Mol. Biol. 19 (2012) 685.
[46] M. Altmeyer, S. Messner, P.O. Hassa, M. Fey, M.O. Hottiger, Molecular mechanism of poly (ADP-ribosyl) ation by PARP1 and identification of lysine residues as ADP-ribose acceptor sites, Nucleic Acids Res. 37 (2009) 3723–3738.
[47] S. Eustermann, H. Videler, J.C. Yang, P.T. Cole, D. Gruszka, D. Veprintsev, D. Neuhaus, The DNA-binding domain of human PARP-1 interacts with DNA single-strand breaks as a monomer through its second zinc finger, J. Mol. Biol. 407 (2011) 149–170.
[48] M.F. Langelier, J.L. Planck, S. Roy, J.M. Pascal, Structural basis for DNA damage-dependent poly (ADP-ribosyl) ation by human PARP-1, Science. 336 (2012) 728–732.
[49] S. Eustermann, W.F. Wu, M.F. Langelier, J.C. Yang, L.E. Easton, A.A. Riccio, J.M. Pascal, D. Neuhaus, Structural basis of detection and signaling of DNA single-strand breaks by human PARP-1, Mol. Cell 60 (2015) 742–754.
[50] L. Liu, M. Kong, N.R. Gassman, B.D. Freudenthal, R. Prasad, S. Zhen, S.C. Watkins, S.H. Wilson, B. Van Houten, PARP1 changes from three-dimensional DNA damage searching to one-dimensional diffusion after auto-PARylation or in the presence of APE1, Nucleic Acids Res. 45 (2017) 12834–12847.
[51] M.E. Fuentes-Perez, M.S. Dillingham, F. Moreno-Herrero, AFM volumetric methods for the characterization of proteins and nucleic acids, Methods 60 (2013) 113–121.
[52] J.D. Steffen, M.M. McCauley, J.M. Pascal, Fluorescent sensors of PARP-1 structural dynamics and allosteric regulation in response to DNA damage, Nucleic Acids Res. 44 (2016) 9771–9783.
[53] R. Alvarez-Gonzalez, M.K. Jacobson, Quantification of poly (ADP-ribose) *in vitro*: Determination of the ADP-ribose chain length and branching pattern, *Poly* (ADP-Ribose) Polymerase, Humana Press, Totowa, NJ 2011, pp. 35–46.
[54] A.E. Fisher, H. Hochegger, S. Takeda, K.W. Caldecott, Poly (ADP-ribose) polymerase 1 accelerates single-strand break repair in concert with poly (ADP-ribose) glycohydrolase, Mol. Cell. Biol. 27 (2007) 5597–5605.
[55] H. Schuhwerk, C. Bruhn, K. Siniuk, W. Min, S. Erener, P. Grigaravicius, A. Krüger, E. Ferrari, T. Zubel, D. Lazaro, S. Monajembashi, K. Kiesow, T. Kroll, A. Bürkle, A. Mangerich, M. Hottiger, Z.Q. Wang, Kinetics of poly (ADP-ribosyl) ation, but not PARP1 itself, determines the cell fate in response to DNA damage *in vitro* and *in vivo*, Nucleic Acids Res. 45 (2017) 11174–11192.
[56] M. De Vos, V. Schreiber, F. Dantzer, The diverse roles and clinical relevance of PARPs in DNA damage repair: current state of the art, Biochem. Pharmacol. 84 (2012) 137–146.
[57] O. Mortusewicz, J.C. Ame, V. Schreiber, H. Leonhardt, Feedback-regulated poly (ADP-ribosyl)ation by PARP-1 is required for rapid response to DNA damage in living cells, Nucleic Acids Res. 35 (2007) 7665–7675.
[58] Q. Chen, M.A. Kassab, F. Dantzer, X. Yu, PARP2 mediates branched poly ADP-ribosylation in response to DNA damage, Nat. Commun. 9 (2018) 3233.
[59] I. Robert, F. Dantzer, B. Reina-San-Martin, Parp1 facilitates alternative NHEJ, whereas Parp2 suppresses IgH/c-myc translocations during immunoglobulin class switch recombination, J. Exp. Med. 206 (2009) 1047–1056.
[60] J. Yélamos, Y. Monreal, L. Saenz, E. Aguado, V. Schreiber, R. Mota, T. Fuente, A. Minguela, P. Parrilla, G. de Murcia, E. Almarza, P. Aparicio, J. Ménissier-de Murcia, PARP-2 deficiency affects the survival of CD4+ CD8+ double-positive thymocytes, EMBO J. 25 (2006) 4350–4360.
[61] J.C. Amé, T. Kalisch, F. Dantzer, V. Schreiber, Purification of recombinant poly (ADP-ribose) polymerases, Methods Mol. Biol. 780 (2011) 135–152.
[62] M. Enoiu, D.T. Long, J.C. Walter, O.D. Schärer, Construction of plasmids containing site-specific DNA interstrand cross-links for biochemical and cell biological studies, Methods Mol. Biol. 920 (2012) 203–219.
[63] T. Lindahl, A. Andersson, Rate of chain breakage at apurinic sites in double-stranded deoxyribonucleic acid, Biochemistry. 11 (1972) 3618–3623.
[64] S.W. Schneider, J. Lärmer, R.M. Henderson, H. Oberleithner, Molecular weights of individual proteins correlate with molecular volumes measured by atomic force microscopy, Pflugers Arch. 435 (1998) 362–367.
[65] Y. Yang, L.E. Sass, C. Du, P. Hsieh, D.A. Erie, Determination of protein–DNA binding constants and specificities from statistical analyses of single molecules: MutS–DNA interactions, Nucleic Acids Res. 33 (2005) 4322–4334.
[66] S.I. Shram, I.G. Rybakova, T. Lazurkina, G.V. Sidorov, G.A. Shilovskiĭ, A.N. Khokhlov, N.F. Miasoedov, Enzymatic synthesis of beta-NAD+ selectively marked with tritium at adenine and its use for determining the activity of poly (ADP-ribose) polymerase, Prikl. Biokhim. Mikrobiol. 35 (1999) 638–646.
[67] P.L. Panzeter, F.R. Althaus, High resolution size analysis of ADP-ribose polymers using modified DNA sequencing gels, Nucleic Acids Res. 18 (1990) 2194.